Taylor & Francis
Taylor & Francis Group

UAS remote sensing missions for rangeland applications

Andrea S. Laliberte[a]*, Craig Winters[b] and Albert Rango[b]

[a]*Jornada Experimental Range, New Mexico State University, Las Cruces, NM 88003, USA;*
[b]*USDA Agricultural Research Service, Jornada Experimental Range, Las Cruces, NM 88003, USA*

Rangelands cover about 50% of the earth's land surface, are in remote areas and have low population densities, all of which provide an ideal opportunity for remote sensing applications from unmanned aircraft systems (UAS). In this article, we describe a proven workflow for UAS-based remote sensing, and discuss geometric errors of image mosaics and classification accuracies at different levels of detail. We report on several UAS missions over rangelands in Idaho and New Mexico, USA, where we acquired 6–8 cm resolution aerial photography and concurrent field measurements. The geometric accuracies of the image mosaics were in the 1–2 m range, and overall classification accuracies for vegetation maps ranged from 78–92%. Despite current FAA regulations that restrict UAS operations to distances within line-of-sight of the UAS, our results show that UAS are a viable platform for obtaining very high-resolution remote sensing products for applied vegetation mapping of rangelands.

Keywords: unmanned aircraft system; UAS; digital camera; photogrammetry; rangelands

1. Introduction

Remote sensing plays an important role in rangeland monitoring and assessment, because rangelands are vast, comprising approximately 50% of the world's land area (Lund 2007), are often difficult to access, and the cost of ground monitoring can be high. Image sensors on satellite or aerial platforms collect earth observation data, and various scales of imagery have been used for rangeland applications to measure vegetation and soil parameters: satellite imagery at various resolutions (Clark *et al.* 2001, Chopping *et al.* 2006, Laliberte *et al.* 2007), videography (Phinn *et al.* 1996, Pickup *et al.* 2000), aerial photography (Yu *et al.* 2006, Stow *et al.* 2008) from piloted aircraft, and ground-based photography (Booth *et al.* 2005).

Aerial photography from unmanned aircraft systems (UAS) can bridge the gap between ground-based rangeland measurements and remotely sensed imagery from piloted aerial and satellite platforms, both in terms of image scale and image acquisition costs. UAS have several advantages over piloted aircraft: UAS can be deployed quickly and repeatedly, for example to assess flooding after sudden

---

*Corresponding author. Email: alaliber@nmsu.edu

rainfalls; there is no risk to an on-board pilot; they can be used to obtain very high-resolution imagery at lower image acquisition costs than with piloted aircraft (Rango *et al.* 2006). UAS also have the potential to be a cheaper platform for acquiring imagery than piloted aircraft, although this is highly dependent on the number of ground crew required by current Federal Aviation Administration (FAA) regulations.

Fine resolution imagery plays an important role in rangeland assessments for the classification of spatial patterns of vegetation and soil patches at multiple spatial scales (Bestelmeyer *et al.* 2006). These fine-scale patterns cannot be resolved with coarser resolution satellite imagery, but are important indicators of erosion risk, wildlife habitat quality and rangeland degradation. Landscape metrics derived from very high resolution imagery can be used in rangeland health assessments and ecosystem models.

Because rangelands are usually located in relatively remote areas and have low population densities, UAS are ideally suited for potentially flying long-duration remote sensing missions over these areas. In general, civil aviation regulatory agencies are more inclined to permit UAS flights, especially low-altitude flights, over remote areas because of less air traffic and reduced danger to people and buildings on the ground (Rango and Laliberte 2010).

Large UAS, such as Ikhana and Global Hawk, have been used or proposed for use in remote sensing in wildfire missions by NASA (Ambrosia and Wegener 2009), while the use of small UAS ($<$ 50 kg) for remote sensing purposes has been less common. This is primarily related to the limited payload capability of small UAS, although recent advances in the miniaturization of sensors, global positioning system (GPS) and inertial measurement unit (IMU) (Patterson and Brescia 2008, Nagai *et al.* 2009) show great promise for UAS as capable remote sensing platforms. Small UAS remote sensing applications have included assessing water stress in crops (Berni *et al.* 2009), crop monitoring (Hunt *et al.* 2010), riparian forest mapping (Dunford *et al.* 2009), and specifically in rangelands, estimation of shrub utilization (Quilter and Anderson 2001) and detection of invasive species (Hardin *et al.* 2007).

At the US Department of Agriculture (USDA), Jornada Experimental Range (JER) in New Mexico, researchers have been investigating the use of UAS for applied rangeland remote sensing for several years (Rango *et al.* 2006, Laliberte and Rango 2009, Laliberte *et al.* 2010). Efforts have focused on developing a workflow for UAS-based aerial photo acquisition, image processing, production of orthomosaics and derivation of classification maps. While many of the image processing steps have their origins in traditional aerial image processing and analysis, some aspects are unique to UAS-acquired imagery, specifically the use of low-cost digital cameras, small image footprints and low accuracy GPS/IMU data. This has resulted in the need to adapt existing approaches or develop new approaches for image processing of UAS-derived imagery.

The objectives of this article are to report on the results of several UAS remote sensing missions, and describe a proven workflow for UAS-based rangeland remote sensing. We will focus specifically on the photogrammetric processing of the images, the geometric accuracies of the orthomosaics and the classification accuracies obtained at different levels of detail. We also address the regulatory issues associated with UAS operations, and discuss the future potential of UAS-based remote sensing for rangeland applications.

2. Methods

2.1 *UAS and sensors*

The small UAS used in our missions was a BAT 3 UAS manufactured by MLB Co. (Mountain View, CA) (Figure 1). The BAT has a 1.8 m wingspan, weighs 10 kg, and has an endurance of 2–6 h. The system is catapult launched from the top of a vehicle, and can be landed manually or autonomously. The GPS-based navigation is based on preprogrammed waypoints, which can be changed and uploaded to the aircraft in real time. The system is equipped with a return-to-home mode if the 900 MHz link or GPS is lost. The UAS can be controlled manually via a 72 MHz link.

The BAT carries two sensors: a colour video camera with optical zoom capability in-flight and live video downlink, and a Canon SD 900 ten megapixel digital camera used for image acquisition for subsequent production of classification maps. Imagery is acquired from an altitude of 214 m above ground. Based on the camera's sensor size of 3072 × 2304 pixels, and a field of view of 53.1°, the image footprint measures 213 m × 160 m, with a nominal ground resolved distance of 6 cm. Images are acquired at 75% forward lap and 40% side lap to ensure sufficient overlap for photogrammetric processing. The images are stored on the camera's 16 gigabyte memory card, and for each image, a timestamp, GPS location, elevation, roll, pitch and heading are recorded by the flight computer. The GPS module (TIM-LP Antaris®) has an update rate of 4 Hz, and the accuracy is 2.5 m. The accuracy of the attitude data from the IMU is rated as $\pm 2°$ for roll and pitch, and $\pm 5°$ for heading.

2.2 *Location of missions and regulatory issues*

Remote sensing missions have been flown over southern New Mexico since 2006 and over southwestern Idaho in 2008 (Figure 2). The New Mexico site is the home base for the UAS operations at the JER, a 78,000 ha field experiment station of the USDA Agricultural Research Service. The western portion of the JER is situated in the National Airspace System (NAS), while the eastern portion adjacent to White

Figure 1. BAT 3 UAS ready to be launched from the catapult. One person holds the launch cord, the second person is on stand-by for manual control, the third person serves as visual observer and performs radio communications.
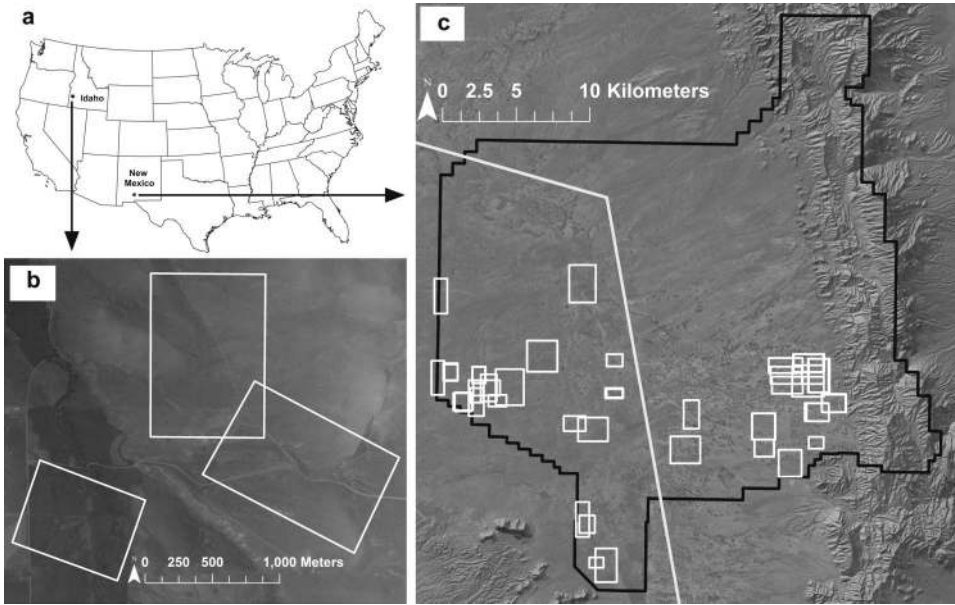
Figure 2. Locations of UAS missions for rangeland remote sensing projects. The overview map (a) shows the locations in Idaho and New Mexico, USA. Flight areas are depicted in white outlines for the 2008 flights in Idaho (b), and for flights conducted at the Jornada Experimental Range (JER) in New Mexico from 2006 to 2010 (c). The black outline represents the JER. The white line in (c) is the boundary between restricted airspace east of the line, and the NAS west of the line.

Sands Missile Range is in restricted airspace. The FAA is charged with regulating UAS operations in the NAS. Those regulations require a Certificate of Authorization (COA) from the FAA (FAA 2010). At the JER, the BAT is operated in the NAS under a COA issued to the New Mexico State University Unmanned Aircraft Systems Flight Test Center, formed through a partnership between the FAA and New Mexico State University. Our flight data are shared with New Mexico State University and FAA to assist with development of standards and regulations for UAS operators. In the restricted airspace, UAS flights are conducted with permission of White Sands Missile Range. In Idaho, flights were conducted under a COA issued to USDA.

Our COA regulations limit flights to 800 m (½ mile) horizontal distance and 300 m (1000 ft) vertical distance to the visual observers. The UAS team consists of a minimum of a pilot in command, internal pilot (ground station operator), external pilot (radio control pilot) and three visual observers. All personnel have a FAA class II medical certificate, the pilots have completed private pilot ground school and the pilot in command has a private pilot's license. Additional personnel include payload and catapult support.

Due to the COA limitations, our flight areas are limited to a length of 1.6 km, while width varies (commonly 0.8–1.6 km). If larger areas have to be covered, multiple flights are conducted, or external pilots and visual observers are moved while keeping the UAS in a line-of-sight holding pattern. In Idaho, three flight areas

were covered in 2008, while in New Mexico, 62 flight areas have been flown since 2006. Overall, we have acquired more than 14,500 images, processed into 65 image mosaics with an average of 234 images per mosaic. In this article, we are reporting on the accuracies of vegetation classifications of image mosaics for two areas in Idaho (65 ha and 83 ha) and two in New Mexico (5 ha, 10 ha), and on geometric accuracy assessments for one Idaho site (116 ha) and one New Mexico site (173 ha).

2.3 *Image processing*

2.3.1 *Orthorectification and mosaicking*

The orthorectification of the imagery was performed using a combination of a customized procedure termed PreSync, followed by orthorectification using Leica Photogrammetry Suite (LPS®) (Erdas 2010). The flowchart (Figure 3) outlines the process. The exterior orientation data, consisting of position (X,Y,Z), and attitude (roll, pitch, heading) data from the BAT's flight computer are not sufficiently accurate to use directly in LPS due to the relatively low-cost GPS and IMU units, and camera/flight data synchronization error of approximately 1 s. PreSync is designed to improve the accuracy of the exterior orientation data, so that orthorectification can be performed in LPS. The approach also minimizes or eliminates the use of manually input ground control points, which are difficult to locate in areas with few distinguishing features and on large numbers of small-footprint images. Inputs to the PreSync procedure include the UAS images of the flight area, initial tie points, initial exterior orientation, a 1 m resolution digital orthoquad (DOQ), a 10 m digital elevation model (DEM) and the camera's interior
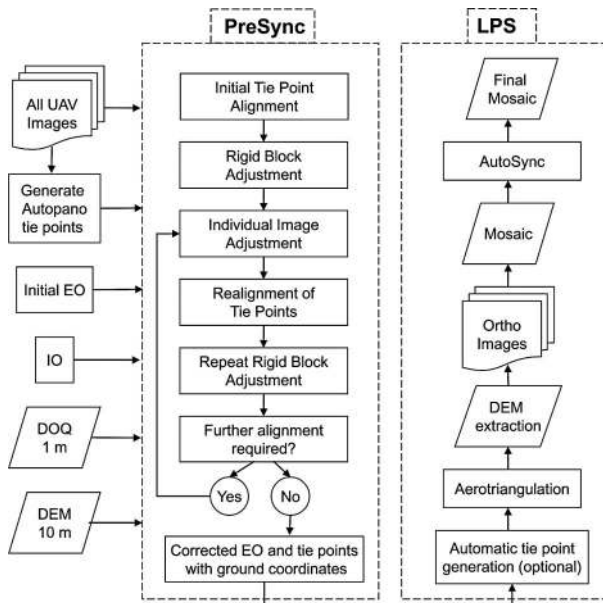

Figure 3. Flowchart of UAS image processing for adjustment of exterior orientation (EO) parameters with the PreSync procedure, and subsequent orthorectification and mosaicking with LPS.

orientation parameters (radial lens distortion, principal point offset, focal length) derived from a camera calibration (Fryer 1996). The initial tie points are derived using Autopano Pro® (Kolor 2009), a program that extracts image tie points automatically without requiring initial exterior orientation data or image-to-flight line matching.

The PreSync workflow consists of combining the reference image (DOQ), the DEM, the exterior and interior orientation parameters, and tie points into a sensor/ environment model, and simulating image acquisition. Simulated imaging projects points from the image plane onto the DEM to locate tie points and to extract a patch of the reference image. Each tie point is evaluated by the variance of its location on multiple images. The reference image patch is transformed to match the sensor array and is evaluated by computing the covariance with the actual sensor image. The exterior orientation is repeatedly adjusted by various means, and is scored based on the tie points and the image covariance. After several iterations, the best scoring value is recorded as the corrected exterior orientation for the image, and used as input to LPS for orthorectification. The main steps of PreSync are (1) initial tie point alignment, (2) rigid block adjustment, (3) individual image adjustment and (4) realignment of tie points. We briefly describe the four steps, but additional detail about the PreSync procedure can be found in Laliberte *et al.* (2008).

In the initial tie point alignment, a mean ground coordinate is assigned to each tie point derived from Autopano Pro, and the exterior orientation of each image is adjusted to minimize the root mean square error (RMSE) of the image's tie points. The next step is a rigid block adjustment of the entire block of images with the goal of maximizing the average covariance of the block. The third step, individual adjustment of each image's exterior orientation value, uses the gradient following search method to maximize image covariance. This reduces relatively large tip-tilt variability between images and lets each image seek its preferred orientation within the local space. The final step is the realignment of tie points while maintaining the tip-tilt corrections from the prior step. If further alignment is required, the rigid block adjustment, and if required, the individual image adjustment, are repeated. The running times for PreSync currently average 2 min per image. The improved exterior orientation values and tie points with ground coordinates are used as input to orthorectification in LPS. Additional automatic tie point generation in LPS is optional to improve the aerotriangulation results.

After orthorectification, we produce an initial image mosaic, which is resampled using the 1 m DOQ as a reference image in the AutoSync module in the Erdas® software (Erdas 2010). This step improves the alignment of the mosaic with existing imagery with little additional time involved, because the tie point collection in AutoSync is automated.

We assessed the positional accuracies of two image mosaics, one in New Mexico for a relative flat site of 173 ha with elevation differences of 14 m (257 UAS images), and the other in Idaho for a topographically more diverse site of 116 ha with elevation differences of 113 m (156 images). For the New Mexico mosaic, we determined RMSEs between image coordinates and coordinates of 72 independent check points (points with a known location) of visible features collected with a Trimble Pro XR® differential GPS unit. For the Idaho mosaic, we obtained coordinates for 591 random points from a 15 cm resolution orthoimage acquired with an UltraCam X digital mapping camera from a piloted aircraft 1 week prior to the UAS flights.

2.3.2   *Image classification*

Developing classification maps from the UAS imagery presents certain challenges compared to using imagery from higher quality mapping cameras. Although the spatial resolution is very high, the spectral and radiometric resolutions obtained from the low-cost consumer camera are relatively low, and the red (R), green (G) and blue (B) bands are highly correlated. A transformation from the RGB space to the intensity-hue-saturation (IHS) space results in reduced band inter-correlation and three additional bands of image information. In the IHS model, the intensity component is separated from the colour information, and the hue and saturation bands relate to how humans perceive colour (Jensen 2005). The use of IHS has been shown to increase classification accuracies with UAS-acquired RGB imagery (Laliberte and Rango 2008), and we routinely use this transformation approach as a pre-processing step.

For the image classification, we used an object-based image analysis (OBIA) approach and the software eCognition® 8 (Definiens 2009). OBIA has seen increasing use over the last 8 years due to the ever increasing resolution of high-resolution satellite imagery, the prevalence of digital aerial imagery, and the bridging of remote sensing and geographic information system (GIS) functionality (Blaschke 2010). The advantages of an OBIA approach versus a pixel-based image analysis approach are greater suitability for very high resolution imagery, the ability to include spectral, spatial and contextual features, and the extraction of ecologically meaningful image objects (Burnett and Blaschke 2003). The general OBIA workflow consists of image segmentation followed by classification of image objects, although in many cases an iterative process is used whereby classification is followed by further segmentation at finer or coarser levels, additional classifications of the image or portions of the image, and merging of objects and/or classes. All the rule sets and algorithms applied to the image are contained in a process tree, which can be saved and easily adapted to other images. This allows for automation or semi-automation of the image analysis workflow.

For the UAS image classifications, the OBIA workflow was adapted to the size of the area due to the limitations on the number of image objects that can be created in eCognition. The limit is between two and five million objects, depending on number of bands, bit depth and complexity of image objects. A typical UAS mosaic with an extent of 1.6 km × 1 km has a file size of two gigabytes, and the maximum number of objects can be exceeded quickly with fine-scale segmentation. Aside from the object number limitation, it is often easier to develop a rule set on a small portion of the image and apply it to additional image subsets than to classify the entire image. With this approach, classification errors are easier to determine, edits are less time consuming and variations in the vegetation communities can be addressed.

For the 5 ha area in New Mexico, the number of objects was not a limitation, and a process tree was developed and applied to the entire image mosaic. For the 10 ha area in New Mexico, which consisted of 18 0.49 ha plots, we developed a process tree on the first plot and applied it to the remaining plots using the workspace feature in eCognition. This allowed for rapid application of the same process tree to multiple individual images in the same work project. A combination of rule-based classification for broader classes and nearest neighbour classification for finer (species-level) classes was used. For the rule-based classification, specific rules were used to define thresholds for the three classes shadow, bare ground and

vegetation. For more detailed classifications at the species-level, field-collected training samples were used for a nearest neighbour classification.

The two areas in Idaho were much larger (65 ha, 83 ha), and we developed the process tree on a 0.25 ha plot surveyed on the ground and classified the image to the structure group level (two bare classes, shrub, grass/forb, shadow) (Laliberte *et al*. 2010). Each of the image mosaics was segmented into tiles, and each tile was segmented at the desired fine scale of analysis and classified using the process tree from the small plot. Rule-based classification was used in these images. Either method, applying the process tree to multiple small images, or tiling a large image and processing each tile in sequence, allows for classifying relatively large UAS image mosaics of sub-decimetre resolution in a semi-automated fashion.

Classification accuracies were assessed by creating error matrices and calculating overall, user's, and producer's classification accuracies, and Kappa statistics (Congalton and Green 2009). For the species-level classifications at the New Mexico sites, the accuracy samples ($n = 762$ and $n = 523$) for the seven classes consisted of image objects, and the accuracy assessments were conducted in eCognition. For the larger sites in Idaho, we used a stratified random point sampling approach with 600 points for five classes, and the accuracy assessment was done in Erdas.

3. Results

3.1 *Geometric accuracies*

Our tests of the geometric accuracies resulted in an RMSE of 0.65 m for the New Mexico image mosaic in the relatively flat area, and an RMSE of 1.14 m for the Idaho image in the area with greater elevation differences (Figure 4). Taking into account the GPS errors for the New Mexico image (84% of the GPS points were in the 30–50 cm range), the approximate geometric accuracy was 1 m. The 15 cm orthoimage used as a reference image for the Idaho site had an accuracy of 80 cm. With this added uncertainty, the accuracy of the Idaho image was approximately 2 m. We acknowledge that the source data for geometric assessment differed, and that neither the differential GPS data nor the coordinates from the orthoimage represent 'true ground' coordinates. Nevertheless, the error assessments offered a reasonable comparison with commonly used reference data, and demonstrated that geometric accuracies can be expected to be lower in areas of greater terrain variation. The AutoSync step in the image processing workflow (Figure 3) improved the geometric accuracy from an RMSE of 1.64 for the initial mosaic output to an RMSE of 0.65 for the New Mexico image, indicating that the AutoSync adjustment offers a relatively quick and effective means of improving the geometric accuracy of the UAS mosaics.

3.2 *Classification approaches*

The classification at the 10 ha New Mexico site was done to the species level using training samples and a nearest neighbour classification. Because the process tree was developed on one plot and applied to subsequent areas of the image, not only the rule base but also the signatures for the training samples were transferred. Even though most species occurred in all plots, some had significantly fewer shrubs than others. Nevertheless, results indicated that the rules and signatures of the process transferred well to other plots. Some edits were required for selected image objects in
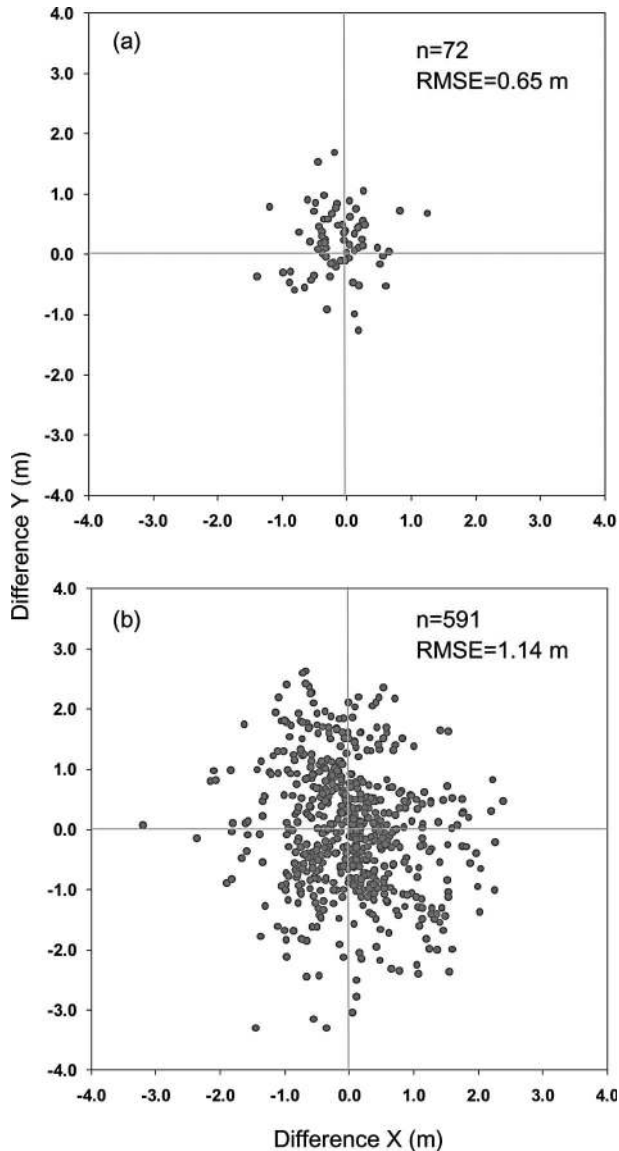
Figure 4.   Geometric accuracies for two UAS mosaics acquired over an area in New Mexico with 14 m elevation difference (a), and over an area in Idaho with 113 m elevation difference (b). The points show differences in the X and Y direction assessed by (a) comparison with check points measured with differentially corrected GPS, and by (b) comparison with coordinates from a 15 cm resolution orthoimage acquired with an UltraCam X digital mapping camera.

each plot, mostly for the litter and black grama classes, which were easily confused. Editing required 5–10 min per plot. We were able to differentiate two shrub species (mesquite, yucca), one sub-shrub (snakeweed) and two grass species (black grama, dropseed) in addition to bare ground, litter, and shadow (Figure 5).

For the larger Idaho sites, a classification at the structure group level (bare ground, shrubs, grass/forb) was performed. Details of the results are shown in Figure 6. Clipping of the UAS mosaic eliminated areas at the image edges which have more distortions. A segmentation into tiles (chessboard segmentation) was the framework for application of the process tree developed on a small subset of the image with representative vegetation (Figure 6(a)). A close-up view of four tiles demonstrates the workflow and results (Figure 6(b)): the upper left tile has been segmented and
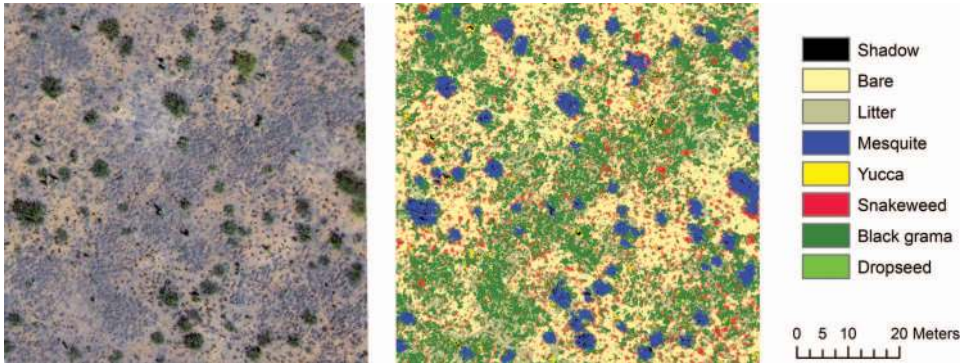
Figure 5.   Portion of UAS image mosaic acquired over rangelands in New Mexico (left) and species-level classification (right). The area shown covers 70 m × 70 m.
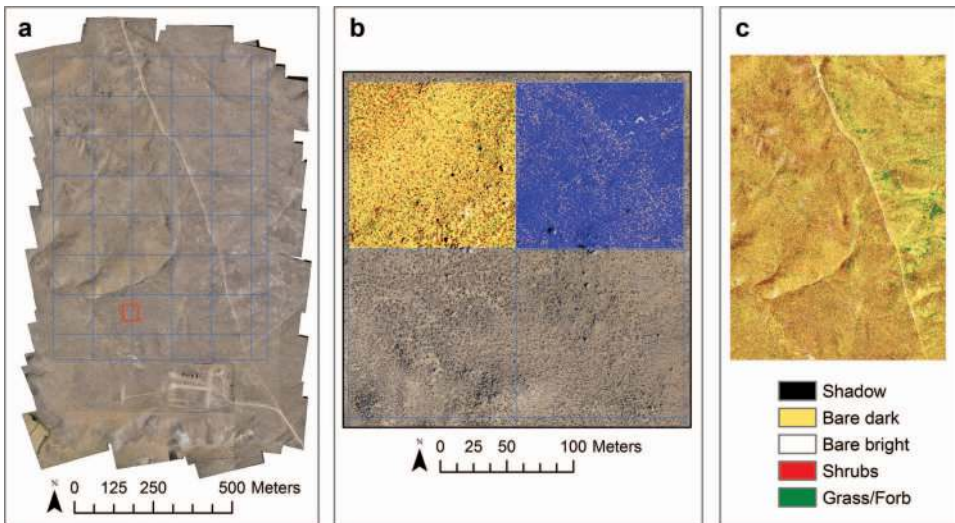

Figure 6.   Classification of UAS image mosaic acquired in Idaho and object-based image analysis workflow using a tiling process. (a) Image mosaic created from 156 images covering 116 ha; the red rectangle represents the 0.25 ha plot where the process tree for the classification was developed. The blue grid represents the segmentation into tiles. (b) Detailed view of the four upper left tiles in (a); the left upper tile has been classified, the right upper tile has been segmented. (c) Final classification. The scale for (c) is identical to (a).

classified, the right upper tile has been segmented to the scale at which the classification will be performed. After that tile has been classified, the next tile is segmented, and so on. The entire classification took 10 h to complete (Figure 6(c)). Visual assessment indicated that the classification rules in the process tree were applicable to the entire image. In contrast to the New Mexico image, no editing was done in the Idaho image due to the larger area and much greater number of segments.

3.3 *Classification accuracies*

The overall classification accuracies obtained with the UAS images are relatively high (78–92%), considering that the images are true colour photography obtained with a low-cost digital camera. The differences in the accuracy results reflect the different objectives for development of classification maps, the extent of areas mapped and the methods of accuracy assessments (Table 1). For the New Mexico sites, the objective was to map relatively small areas at the species level, while for

Table 1. Classification accuracies obtained for object-based classifications of UAS image mosaics acquired over arid rangelands at two sites in Idaho and two sites in New Mexico.

Site and classes	Producer's accuracy (%)	User's accuracy (%)	Number of samples[a]	Overall accuracy (%)	Kappa index
Idaho site 1, 65 ha			Total 600	88	0.82
Shadow	70	91	30		
Bare bright	82	100	22		
Bare dark	98	88	326		
Grass/Forb	78	79	79		
Shrubs	80	96	143		
Idaho site 2, 83 ha			Total 600	83	0.73
Shadow	85	95	22		
Bare bright	87	100	31		
Bare dark	85	91	354		
Grass/Forb	83	62	70		
Shrubs	80	75	123		
NM site 1, 10 ha			Total 762	78	0.64
Bare	78	75	70		
Litter	76	95	115		
Mesquite	99	81	165		
Yucca	48	56	109		
Snakeweed	46	82	113		
Black grama	84	31	94		
Dropseed	87	25	96		
NM site 2, 5 ha			Total 523	92	0.90
Bare bright	94	99	77		
Bare dark	98	96	93		
Mesquite	99	95	83		
Snakeweed	85	96	44		
Burrograss	97	95	82		
Tobosa dense	83	75	77		
Tobosa sparse	90	91	67		

[a]For the two Idaho sites, the samples consisted of points, while for the two New Mexico sites, the samples consisted of image segments.

the Idaho sites, structure groups were mapped over relatively larger areas. We also used two different methods of accuracy assessment. The training and accuracy samples in the New Mexico sites were based on image segments. In the Idaho sites, no training samples were used because classification was rule-based, and the accuracy samples were based on points due to the much larger image extent. For those reasons, direct comparisons of accuracies between all sites should not be attempted.

The two Idaho sites can be compared, because the same classes were mapped over areas of similar size, and both accuracy assessments consisted of 600 point samples. While shrubs and bare ground had high accuracies in both sites, it was apparent that the grass/forb class presented a greater challenge, resulting in lower accuracies. This can be related to the time of image acquisition. In September, this area of Idaho is relatively dry, and grasses contain more senescent than green vegetation, resulting in confusion between grasses and shrubs and grasses and the bare dark class.

Although the two New Mexico sites shared some of the same species, the sites differed in terms of vegetation complexity and desired mapping objective. Site 2 (the 5 ha site) had spectrally more unique classes as well as a greater density of training and test samples. This site had a much higher accuracy for snakeweed, and considering that the bare class was split into bare bright and bare dark, the accuracies were relatively high compared to the bare class in New Mexico site 1 (the 10 ha site). Another reason for the lower accuracy at site 1 was the inclusion of the litter class. A specific mapping objective at site 1 was to determine the separability between litter and other classes. As it turned out, litter was confused with black grama grass, with some snakeweed plants that contained a mixture of green and senescent plant material, and with dropseed, a bunchgrass that occurs in very small patches. We did observe that at both New Mexico sites, mesquite had comparable producers and users accuracies, very likely attributable to the fact that mesquite is a relatively large shrub and less likely confused with other classes. Some of the differences between users and producers accuracies for a given species at New Mexico site 1 likely reflect the limit of separability between species and litter that can be obtained with this type of imagery.

4. Discussion and conclusions

In this article, we have described a workflow for UAS-based rangeland remote sensing, and reported on accuracy assessments of resulting orthomosaics and classification maps. Approaches used in the processing of imagery from piloted aerial photography missions can be applied, although the methods require adaptations to the unique challenges that are often associated with UAS-acquired imagery: low accuracy telemetry data for some UAS with low-cost GPS units, use of consumer digital cameras and potentially large image mosaic files. The low accuracy of the exterior orientation data obtained with small UAS usually preclude either direct georeferencing used with higher accuracy imagery (Jacobsen 2002), or immediate input into commercial photogrammetry software. This has led many to develop custom applications for processing of UAS imagery (Du *et al.* 2008, Wilkinson *et al.* 2009, Zhou 2009). Our approach is unique, because the PreSync module is aimed at improving the exterior orientation values, and we take advantage of existing software for tie point detection and final orthorectification. The PreSync workflow

has been tested to date on 65 image mosaics of arid rangelands with few distinguishing features. Considering the resolution difference between the UAS images and the 1 m DOQ images used for matching, the process has performed well, even though the DOQs have been up to 4 years older than the UAS images. This time difference has not affected the processing of images from relatively slowly changing rangelands. In areas of greater change over time, such as hayfields, we have observed some difficulties in image matching.

Because our approach does not require much operator interaction, an orthorectified image mosaic of 250 images can be obtained approximately 2 days after the flight. The geometric accuracies of the image mosaics are suitable for routine rangeland monitoring purposes, and allow for relating image information to ground-based vegetation measurements.

While the low radiometric and spectral resolution of low-cost digital cameras has its limits in terms of classification products, we have shown that by using a conversion to the IHS space and OBIA, we can produce structure-level or species-level thematic maps for rangeland assessment at relatively high accuracies. We have shown in a related study that a plot-based remote sensing analysis of UAS images for percent cover values was more efficient than a ground-based measurement approach when more than eight plots were analysed (Laliberte *et al.* 2010). The segmentation of a mosaic into smaller, manageable tiles that are subsequently processed with an identical rule-base, offers an approach to classify large image files that would otherwise exceed the maximum number of segments in the OBIA approach. While we executed the tiling within an eCognition project using a chessboard segmentation, the Enterprise version of the software can manage tiling and stitching on a server, thus greatly increasing the processing ability.

The classification accuracies we obtained were highly dependent on the level of detail, number of classes, size of area and specific mapping objectives, not unlike any other mapping project. However, the results are promising and certainly show that a UAS equipped with a low-cost digital camera can serve as a viable remote sensing platform for rangeland assessment. While certain classes, such as litter, may be difficult to distinguish given the camera used, structure level mapping is certainly possible at relatively high accuracies. Remotely sensed estimates of non-vegetated areas, shrub and grass cover are tied to soil and site stability, watershed function, and biotic integrity, all rangeland attributes commonly monitored with ground-based methods (Herrick *et al.* 2005). Using a UAS to obtain estimates of land cover parameters at the landscape scale allows us to then focus on specific areas that require ground measurements at a greater level of detail.

FAA rules for operating a UAS in the NAS currently have limitations for large-area rangeland assessments with UAS (Rango and Laliberte 2010). The ability to fly autonomously at relatively large distances from base operations is one of the advantageous of UAS and could potentially be exploited by public land management agencies to monitor vast and remote rangelands. However, current regulations (FAA 2008) limit UAS flights to within line-of-sight, requiring the use of visual observers or chase aircraft. In April 2009, the small UAS aviation rulemaking committee (ARC) submitted their recommendations to the FAA. Due to their low cost and operating expenses, and suitability for remote sensing, small UAS are predicted to have the fastest growth of any UAS. It is anticipated that small UAS will be regulated separately from large UAS in the future, hopefully allowing for broader use in natural resource applications.

Our ongoing research is focused on investigating new sensors and novel image analysis approaches for UAS-acquired imagery. Aside from evaluating classification accuracies and refining methods for processing and analysing large image files, UAS imagery acquired at the JER is currently being used to adapt field sampling to very high resolution imagery, derive parameters for a deterministic hydrologic model, support repetitive data analysis for a phenology pilot study, assist in evaluation of disturbance experiments and contribute high resolution information for archaeological studies.

We are currently integrating into the UAS a multispectral camera that acquires 10-bit radiometric data in six narrow bands ranging from blue to near infrared. This imagery will support radiometric correction and will allow for better species differentiation. In addition, we are developing methods to fuse the optical data with dense surface models generated from the UAS images for derivation of vegetation heights. Plans for testing of additional sensors are underway. We encourage the FAA to develop UAS regulations that will allow for applying image processing and analysis methods developed on smaller areas to the landscape scale, so that UAS-based remote sensing can be further integrated into rangeland assessments.

Acknowledgements

References

Ambrosia, V.G. and Wegener, S.S., 2009. Unmanned airborne platforms for disaster remote sensing support. *In*: P.-G.P. Ho, ed. *Geoscience and remote sensing*. Vukovar, Croatia: In-Tech, 91–114.

Berni, J.A.J., *et al.*, 2009. Thermal and narrowband multispectral remote sensing for vegetation monitoring from an unmanned aerial vehicle. *IEEE Transactions on Geoscience and Remote Sensing*, 47 (3), 722–738.

Bestelmeyer, B.T., *et al.*, 2006. A multi-scale classification of vegetation dynamics in arid lands: what is the right scale for models, monitoring, and restoration? *Journal of Arid Environments*, 65, 296–318.

Blaschke, T., 2010. Object based image analysis for remote sensing. *ISPRS Journal of Photogrammetry and Remote Sensing*, 65, 2–16.

Booth, D.T., *et al.*, 2005. Image analysis compared with other methods for measuring ground cover. *Arid Land Research and Management*, 19, 91–100.

Burnett, C. and Blaschke, T., 2003. A multi-scale segmentation/object relationship modelling methodology for landscape analysis. *Ecological Modelling*, 168 (3), 233–249.

Chopping, M., *et al.*, 2006. Mapping shrub abundance in desert grasslands using geometric-optical modeling and multi-angle remote sensing with CHRIS/Proba. *Remote Sensing of Environment*, 104, 62–73.

Clark, P.E., Seyfried, M.S., and Harris, B., 2001. Intermountain plant community classification using Landsat TM and SPOT HRV data. *Journal of Range Management*, 54, 152–160.

Congalton, R.G. and Green, K., 2009. *Assessing the accuracy of remotely sensed data: principles and practices*. Boca Raton: CRC Press.

Definiens, 2009. *eCognition developer 8.0 user guide*. Munich: Definiens AG.

Du, Q., *et al.*, 2008. Automatic registration and mosaicking for airborne multispectral image sequences. *Photogrammetric Engineering and Remote Sensing*, 74 (2), 169–181.

Dunford, R., *et al.*, 2009. Potential and constraints of unmanned aerial vehicle technology for the characterization of Mediterranean riparian forest. *International Journal of Remote Sensing*, 30 (19), 4915–4935.

Erdas, 2010. *Erdas 2010 field guide*. Norcross, GA: Erdas.

Federal Aviation Administration (FAA), 2008. *Interim operational approval guidance 08–01: unmanned aircraft systems operations in the U.S. National Airspace System, FAA Aviation Safety Unmanned Aircraft Program Office* [online]. Available from: http://www.faa.gov/about/initiatives/uas/reg/media/uas_guidance08-01.pdf [Accessed 20 July 2010].

Federal Aviation Administration (FAA), 2010. *Unmanned aircraft systems (UAS), regulations and policies, FAA Aviation Safety Unmanned Aircraft Program Office* [online]. Available from: http://www.faa.gov/about/initiatives/uas/reg/ [Accessed 20 July 2010].

Fryer, J.G., 1996. Camera calibration. *In*: K.B. Atkinson, ed. *Close-range photogrammetry and machine vision*. Scotland: Whittles Publishing, 156–179.

Hardin, P.J., *et al.*, 2007. Detecting squarrose knapweed (Centaurea virgata Lam. Ssp. squarrosa Gugl.) using a remotely piloted vehicle: a Utah case study. *GIScience and Remote Sensing*, 44 (3), 1548–1603.

Herrick, J.E., *et al.*, 2005. *Monitoring manual for grassland, shrubland and savanna ecosystems. Quick start*. Vol. I. *Design, supplementary methods and interpretation*. Vol. II. Las Cruces, NM: USDA-ARS Jornada Experimental Range.

Hunt, E.R., *et al.*, 2010. Acquisition of NIR-green-blue digital photographs from unmanned aircraft for crop monitoring. *Remote Sensing*, 2, 290–305.

Jacobsen, K., 2002. Calibration aspects in direct georeferencing of frame imagery. *Pecora 15/Land Satellite Information IV/ISPRS Commission I/FIEOS 2002*, 10–15 November 2002. [unpaginated CD-ROM]. Denver, CO: ASPRS.

Jensen, J.R., 2005. *Introductory digital image processing: a remote sensing perspective*. Upper Saddle River: Prentice-Hall.

Kolor, 2009. *Autopano pro version 2.0.2* [online]. Available from: http://www.autopano.net [Accessed 18 July 2010].

Laliberte, A.S., Fredrickson, E.L., and Rango, A., 2007. Combining decision trees with hierarchical object-oriented image analysis for mapping arid rangelands. *Photogrammetric Engineering and Remote Sensing*, 73 (2), 197–207.

Laliberte, A.S., Winters, C., and Rango, A., 2008. A procedure for orthorectification of sub-decimeter resolution imagery obtained with an unmanned aerial vehicle (UAV). *ASPRS Annual Conference Proceedings*, 28 Apr–2 May 2008. [unpaginated CD-ROM]. Portland, OR: ASPRS.

Laliberte, A.S. and Rango, A., 2008. Incorporation of texture, intensity, hue, and saturation for rangeland monitoring with unmanned aircraft imagery. *In*: G.J. Hay, T. Blaschke, and D. Marceau, eds. *The International Archives of the Photogrammetry, Remote sensing, and Spatial information sciences, GEOBIA 2008*, 5–8 August 2008. [unpaginated CD-ROM]. Vol. XXXVIII-4/C1. Calgary, AB: ISPRS.

Laliberte, A.S. and Rango, A., 2009. Texture and scale in object-based analysis of sub-decimeter resolution unmanned aerial vehicle (UAV) imagery. *IEEE Transactions of Geoscience and Remote Sensing*, 47 (3), 761–770.

Laliberte, A.S., *et al.*, 2010. Acquisition, orthorectification, and object-based classification of unmanned aerial vehicle (UAV) imagery for rangeland monitoring. *Photogrammetric Engineering and Remote Sensing*, 76 (6), 661–672.

Lund, H.G., 2007. Accounting for the world's rangelands. *Rangelands*, 29 (1), 3–10.

Nagai, M., *et al.*, 2009. UAV-borne 3-D mapping system by multisensor integration. *IEEE Transactions on Geoscience and Remote Sensing*, 47 (3), 701–708.

Patterson, M.C.L. and Brescia, A., 2008. Integrated sensor systems for UAS. *Proceedings of the 23rd Bristol International Unmanned Air Vehicle Systems (UAVS) Conference*, 7–9 April 2008. Bristol, UK: University of Bristol. 19.1–19.13.

Phinn, S., *et al.*, 1996. Biomass distribution mapping using airborne digital video imagery and spatial statistics in a semi-arid environment. *Journal of Environmental Management*, 47, 139–164.

Pickup, G., Bastin, G.N., and Chewings, V.H., 2000. Measuring rangeland vegetation with high resolution airborne videography in the blue-near infrared spectral region. *International Journal of Remote Sensing*, 21 (2), 339–351.

Quilter, M.C. and Anderson, V.J., 2001. A proposed method for determining shrub utilization using (LA/LS) imagery. *Journal of Range Management*, 54, 378–381.

Rango, A., *et al.*, 2006. Using unmanned aerial vehicles for rangelands: current applications and future potentials. *Environmental Practice*, 8, 159–168.

Rango, A. and Laliberte, A.S., 2010. Impact of flight regulations on effective use of unmanned aircraft systems for natural resources applications. *Journal of Applied Remote Sensing*, 4, 043539.

Stow, D., *et al.*, 2008. Monitoring shrubland habitat changes through object-based change indentification with airborne multispectral imagery. *Remote Sensing of Environment*, 112, 1051–1061.

Wilkinson, B.E., *et al.*, 2009. A new approach for pass-point generation from aerial video imagery. *Photogrammetric Engineering and Remote Sensing*, 75 (12), 1415–1423.

Yu, Q., *et al.*, 2006. Object-based detailed vegetation classification with airborne high spatial resolution remote sensing imagery. *Photogrammetric Engineering and Remote Sensing*, 72 (7), 799–811.

Zhou, G.Q., 2009. Near real-time orthorectification and mosaic of small UAV video flow for time-critical event response. *IEEE Transactions on Geoscience and Remote Sensing*, 47 (3), 739–747.